Chapter 6

Detection of Biomarkers for Respiratory Distress in Exhaled Breath Condensate

Our understanding of asthma was fundamentally altered when it was revealed to be not a single disease but rather a variety of phenotypes involving various tissues and molecular factors. The exact nature of the pulmonary inflammation is phenotype-specific, and a lack of information about the state of the respiratory system during an episode can hinder a diagnosis. A library of biological markers of pulmonary inflammation are being used to try to probe these different disease states, but specimen collection becomes a challenge when typical methods such as bronchoalveolar lavage, sputum induction, and bronchoscopy pose health threats and significant discomfort to the patient. Other specimen types, such as urine or plasma, offer only information about systemic inflammation.

Exhaled breath condensate (EBC) has emerged as a non-invasive alternative to these methods, where the aerosols in breath are condensed and collected in the liquid phase [141, 142]. This method is an effective and way to sample both volatile and non-volatile species within the respiratory tract, and has proven to be useful tool in asthma research due to its ease and repeatability. Specimen collection typically takes 10 minutes and, unlike with urine or plasma, offers localized information about the lungs at a specific point in time. This method has played an integral role in the study of two particular classes of biological molecules that describe respiratory conditions.

6.1 Biomarkers for Oxidative Stress

One such group of biomarkers is the leukotrienes (LTs). They are the result of arachidonic acid breakdown in the cell membrane first by 5-lipoxygenase (5-LOX) and then by another enzyme. Specifically, leukotriene LTC_4 synthase produces the cysteinyl leukotrienes, which include LTC_4, LTD_4, and LTE_4, and leukotriene A_4 hydrolase produces LTB_4. They are small molecules (molecular weight ≈330 g/mol) and are understood to be proinflammatory factors released by mast cells and eosinophils that are capable of contracting airway smooth muscles and increasing mucus secretion and vascular permeability. Elevated levels of the cys-LTs have been found in asthmatic adults and children [143, 144, 145], and Balanzá et al. [146] demonstrated a 20-fold increase in LTB_4 in children with persistent asthma, but only a 2-fold increase in children with episodic asthma.

Another common species found in conveniently high concentrations in EBC are isoprostanes, a class of small molecules (molecular weight ≈350 g/mol) that result from the free radical-catalyzed peroxidation of arachidonic acid as opposed to the naturally-occuring cyclooxygenase-catalyzed peroxidation [147]. For this reason, they make excellent markers for the oxidative stress level in the respiratory system when collected in the EBC. The prevalent regioisomer of this class is 8-isoprostane (8ip), also referred to as 15-F_{2t}-isoprostane, 8-epi PGF2α, and isoprostane-$F_{2\alpha}$-III. It is present in EBC at elevated levels in patients with asthma [148], cystic fibrosis [149], and sleep apnea [150] as well as in patients who smoke [151]. Interestingly, the same 2010 study by Balanzá et al. [146] that reported distinctly different LTB_4 levels according to episodic or persistent asthma also reported a disproportionately smaller difference in 8ip levels between the two groups, implying that a combination of these two markers could provide even more information about nature of the condition for a given patient.

It is rather fortunate that species such as leukotrienes and 8-isoprostane are present at such high concentrations in EBC, but it is unclear whether more reliable or informative biomarkers are present below the detection limits of those methods currently used or whether subpopulations could be better resolved with more sensitive analytical methods. Zanconato et al. observe in their 2004 study that 8-isoprostane levels in the EBC of a population of children with unstable asthma appears bimodal, suggesting the "heterogeneity

Table 6.1: Local Concentrations of 8-isoprostane in the Body [3]

Organ	Concentration
Liver	8-114 ng/g
Kidney (urine)	57-390 ng/g
Blood	20-80 pg/mL
Lung	5-60 pg/mL

of asthma phenotypes in subjects with difficult-to-control asthma" [145]. Analytical methods are limited for these measurements. Small molecules such as leukotrienes and 8-isoprostane are typically measured with either gas chromatography/mass spectrometry (GC/MS), liquid chromatography/mass spectrometry (LC/MS), or enzyme immunoassays (EIAs), but studies looking at the proteins found in the EBC use EIAs, flow cytometry, or enzyme-linked immunosorbent assays (ELISAs) [141]. The published limits of detection for all of these methods are between 1 and 10 pM. Unfortunately, the levels present in healthy subjects is no more than a factor of 2-4 higher than that limit (see Table 6.1). While EBC gives researchers a valuable tool to collect specimens that can accurately describe respiratory health, there remains a clear need to evaluate these samples with more sensitive techniques in order to search for biomarkers that current methods cannot detect. Increased sensitivity would make it possible to mine these samples for as much information as possible.

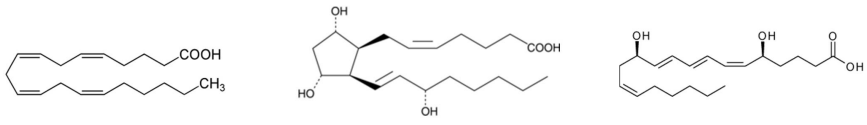

(a) Arachidonic Acid (b) 8-isoprostane (c) Leukotriene B4

Figure 6.1: The structures of arachidonic acid and two of its derivatives most useful as biomarkers of oxidative stress

6.2 Whispering Gallery Mode Optical Biosensors

Whispering gallery mode (WGM) optical biosensors have demonstrated extraordinary sensitivity for detecting the specific binding of proteins to their surfaces via immobilized antibodies [1, 6]. These round, microscale, dielectric devices trap light circulating around their periphery. Their smooth walls continually steer the light inward and minimize losses. When the trip around the periphery is equal to an integer number of optical cycles, the light is in phase with itself and may undergo constructive interference. The intensity of this resonant light grows until the input rate is balanced by the cumulative losses of the resonator. The quality factor, Q, the figure of merit often used to characterize loss in a resonator, is the ratio of the energy stored in the cavity, W, to the energy lost per optical cycle. It may be expressed in terms of the resonant frequency, ω_R, and the power coupled into the resonator, P_C, as $Q = \omega_R \frac{W}{P_C}$. At steady state, $P_C = P_D$, where P_D is the readily measured dissipated power. Though a number of mechanisms exist through which light may be lost from the resonator, the scattering due to surface roughness at the interface between the resonator and surrounding medium and the absorption of light by these materials are the two most significant.

Microtoroidal resonators have demonstrated quality factors of $> 10^8$ in water, and have been used to develop label-free bioassay sensors with attomolar (10^{-18} M) limits of detection for proteins [1] and small molecules [152] in both buffer and complex biological media [1]. While other devices, such as surface plasmon resonance (SPR), have acheived picomolar sensitivity, only the WGM optical biosensor has demonstrated label-free detection with this extreme sensitivity. The markers of interest here are much smaller than the species commonly studied in the literature. The present work examines the potential of the WGM optical biosensor for the previously unexplored class of diagnostic molecules.

The established performance of WGM biosensors [72, 73, 74] makes them an excellent candidate for use in low-concentration medical diagnostic and analytical measurements. Here we demonstrate that these devices can exceed the detection limits of current methods for sensing small molecule biomarkers that are found in EBC, thereby expanding the value of that non-invasive sampling method and accelerating its adoption into standard medical practice. As there appears to be no standard means of analysis for quantifying biomarkers of oxidative stress in the respiratory track [3], this exercise stands to present a technique to both unify and

improve this process.

6.3 Detection of Model Biomarkers

To demonstrate the utility of WGM biosensors for detection of biomarkers in biological samples we choose as our analytes 8ip (M_w 350 g/mol) and the small protein Interleukin-2 (M_w 15300 g/mol), species with molecular weights that differ by nearly two orders of magnitude. While we discuss the significance and convenience of 8ip, it is worth noting that proteins in the interleukin family have been detected in EBC and may also serve as biomarkers for interrogating respiratory distress [153, 141]. These cytokines serve as intercellular signalling molecules during inflammation and immune response. Interleukin-2 [14] in particular has been used many times over as a model system with which to validate biosensor performance [1, 54], partly because monoclonal antibodies are available for its human variant.

The experiments that demonstrated the extreme sensitivity of the microtoroidal WGM sensor employed a New Focus Velocity^{TM}laser operating at a wavelength of $\approx$ 680 nm. Unfortunately, that mechanically-tuned laser was too delicate for reliable use in routine sensing, so an alternative source was sought for this application. Yariv and coworkers [154] have developed a current-tuned distributed-feedback (DFB) laser that is much better suited for use in the long-term development of WGM biosensing instruments. The DFB laser produces a linear sweep in optical frequency by using an interferometer to combine the laser output with a delayer version of itself. As the frequency is swept, the light that is transmitted through different lengths of optical fiber differ in phase, producing an optical “beat" pattern when combined and sent to a photodetector. The resulting sinusoidal signal is used as a feedback signal to control the current source responsible for tuning the optical frequency. Further details of this laser system are provided in [154].

This laser is not continuously tuned in a symmetric sawtooth patthern like the more common external cavity laser (ECL), which is described in Chapter 3 and illustrated in Fig. 6.2. Instead, it is swept in a linear frequency “chirp," as illustrated by the blue line. This optoelectronic swept frequency laser (OSFL) represents a considerable improvement over ECLs due to its robust design that has no moving parts. Building

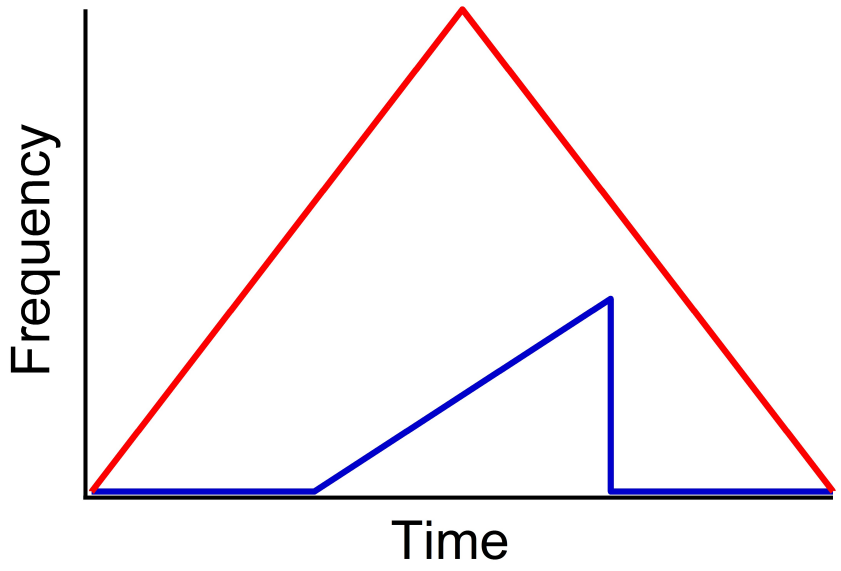

Figure 6.2: Typical frequency scan profile shape for external cavity laser (red) and chirp laser (blue). Note that the ECL has a wider tuning range; however, the OSFL laser has no moving parts so it may attain a far greater range of scan rates.

one also costs 10-40% of what most commercially available ECLs cost. Chirp lasers are limited by the wavelength and linewidth laser, however. Laser diodes that operate at visible wavelengths that are suitable for current tuning are rare because, unlike for near-infrared wavelengths such as 1310 nm and 1550 nm used in telecommunications, there is no great industrial need for them. Moreover, the inexpensive near-infrared laser diodes lack the diffraction gratings used in ECLs to produce narrow linewidths of < 1 MHz, increasing the noise of biosensing data collected collected using OSFLs relative to the alternative. While efforts to build an acceptable OSFL laser with output of $\lambda < 1310$ nm to reduce absorptive losses due to water are ongoing, the experiments described below were performed using a 1310 nm OSFL.

Experimental Methods

In performing sensing experiments with Interluekin-2 (IL2) and 8-isoprostane (8ip) we hope to clarify two performance characteristics of WGM sensors: (i) the limit of detection for each type of analyte, and (ii) the repeatability of the endpoint measurement that might be used to quantify the presence of the analyte

in a biological sample. The first measurement comes down to the straightforward task of identifying the concentration of analyte below which the sensor gives a signal indistinguishable from noise (see Section 2.4). The second is more difficult because it requires excellent control over the sensor fabrication process. For microtoroidal WGM biosensors, this process involves lithographically definining a silica disk, gas-phase etching to remove silicon some from beneath that disk, and reflowing the disk using a CO_2 laser. This process is discussed in greater detail in Chapter 3. Each step involves variability that is compounded throughout the process, all but eliminating the chances of being able to establish repeatability using different devices. Instead, we focus here on using a single sensor and regenerating its surface between experiments.

As a first step toward accomplishing these goals, we conduct a series of experiments using a microtoroidal WGM biosensor to detect Interleukin-2 in buffer by immobilizing monoclonal anti-IL2 on the sensor surface. The injection port was a 23-gauge stainless steel tube, connected to a syringe mounted on a syringe pump. The injection tube was placed roughly 5 mm away from and aimed directly at the toroid being used in the experiment such that the tapered optical fiber waveguide was between the injection tube and the sensor. An open flow cell was constructed by attaching a glass coverslip cleaned in pirhana solution (30 vol% standard hydrogen peroxide solution, 70 vol% pure sulfuric acid for 60 minutes followed by a rinse in ultrapure water) to a stainless steel sample holder using minimal superglue. The glass coverslip is glued to and cantilevered off of a 1 mm tall spacer made from a small piece of a silica microscope slide cut to be as wide as the sample holder. A chip with a linear array of toroidal resonators was also glued to the stainless steel holder.

After waiting 30-60 minutes for the cyanoacrylate adhesive to react completely with atmospheric water, the sample holder was mounted on a piezo block for accurate positioning of the resonators with respect to the waveguide. The flow cell was flooded carefully by hand using a micropipette, adding buffer simultaneously on both sides of the taper to minimize the risk that capillary forces and water surface tension would break the waveguide as the cell filled. The volume of the flow cell varies each time one is made, but most are between 400-600 μL. A flow rate of 50 μL/min was used for all experiments.

Light from the OSFL was coupled into an optical fiber containing a tapered section to facilitate coupling of light into the optical resonator sensor. The tapered optical fiber waveguide was fabricated by pulling a piece

of stripped and cleaned fiber over a hydrogen flame. The light transmitted through the waveguide was sent to a low-noise photodetector (Thorlabs, 200 MHz) that was connected to an oscilloscope (Tektronix TDS-2024B, 2000 points per scan). The pulse function sent to current source responsible for tuning the OSFL output wavelength was used to trigger the oscilloscope. Data collection involved the capture of entire transmission spectra, which facilitated the measurement of coupled power, Q, and $\Delta\lambda_R$. Raw data was acquired with a time resolution of ≈ 1 second using a script written in Igor 6.1 (Wavemetrics) to communicate with the oscilloscope. A constant coupling was maintained during the experiment through manual manipulation of the piezo controller according to live feedback from the depth of the Lorentzian trough in the transmission spectrum shown on the oscilloscope.

Protein solutions were made in a buffer consisting of 100 mM 4-(2-hydroxyethyl)-1-piperazine ethanesulfonic acid (HEPES), 100 mM NaCl, and a pH of 7.5 that was stored at room temperature. Phospate buffered saline, though a popular and convenient simulation of biological conditions, were unsuitable for our experiments as the phosphate absorbs light far more efficiently at 1310 nm than at 633 nm, leading to artifacts in the data. Protein stocks were stored in 20 μm aliquots at -20 °C, and solutions were maid daily and stored at 4 °C until 30 minutes before an experiment to allow for thermal equilibration at room temperature. The flow cell was flushed with 3 mL of buffer before any experiments were performed to remove any accumulated dust particles that may have been deposited during the the construction and subsequent curing of the flow cell structure.

Surface functionalization was achieved by first applying a nonspecifically-bound layer of Protein G to the bare silica surface. A 100 nM solution was introduced into the cell until the sensor showed a new steady-state value of λ_R to reflect the saturation of the sensor surface. The cell was then rinsed with 3 mL of buffer before flowing a 100 nM solution of antibody into the cell. Protein G is known to bind to the FC region of an antibody, ensuring that the molecular recognition regions of the molecules are oriented so that they may specifically bind their antigen. After the surface is saturated with antibody, the cell is rinsed again. The monoclonal antibody used for IL-2 was purchased from Invitrogen while the polyclonal antibody for 8ip was purchased from Cayman Chemicals.

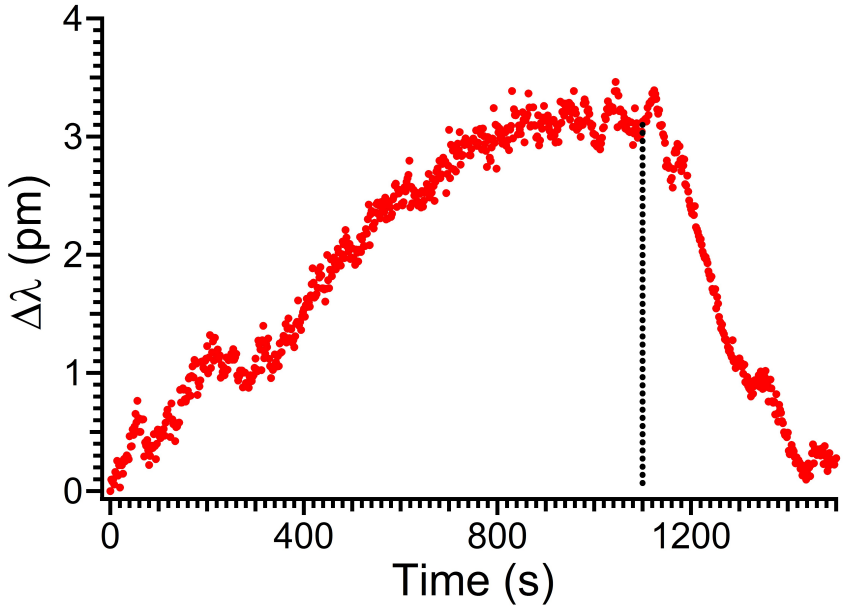

Figure 6.3: Typical sensor response for a microtoroid resonator in water at 1310 nm exposed to 50 μL/min flow of water. The dotted line marks the point at which flow was shut off.

Preliminary Results

In all experiments, we observed a sensor response upon flowing of buffer into the cell without protein present to adsorb to the device. Even when ultrapure water is flowed at 50 μL into the cell, we observe a reversible increase in the resonant wavelength, as demonstrated in Fig. 6.3. It is well-known that water absorbs light efficiently at 1310 nm, and the resulting heating is likely behind this effect. Just as described in Chapter 4 for the case of mass transfer, a temperature boundary layer forms in the region close to the sensor where thermal diffusion is the dominant mode of energy transfer and convection is locally negligible due to viscous forces. We have shown that the thickness of this region, δ, decreases with increasing flow velocity *or* decreasing size of the flow obstacle.

Increasing the inlet flow rate might then produce a thinner layer over which convection is unable to rinse away the water warmed by the optical field than at lower flow rates. Since the thermal flux q obeys Fourier's Law according to $q = -\kappa_T \nabla T$, where κ_t is the thermal conductivity and T is the temperature, the thinner boundary layer that results from an increased inlet flow rate will also lead to an increased temperature

gradient at the surface of the resonator. Ultimately, heat will be better removed from the warming resonator under these conditions than if the inlet flow were small. Any change in temperature T of a material is accompanied by a change in refractive index n according to the thermo-optical constant $\frac{dn}{dT}$. As a result, the sensor will experience a change in the resonant wavelength when the temperature around the the device is perturbed by flow according to

$$\frac{\Delta\lambda_R}{\lambda_R} = \frac{\Delta n_{eff}}{n_{eff}} = \frac{\frac{dn}{dT}\Delta T}{n_{eff}}. \tag{6.1}$$

The thermo-optical constant of water is -9.9×10^{-5} K^{-1} [135], and any increase in the water temperature will produce a decrease in the resonant wavelength.

According to Eq. (6.1), this would suggest a blue shift in the resonance in response to absorption of light by the water, however this effect can only be observed when comparing the λ_R with the value measured in the limit of zero absorption. Instead, multiple processes are occurring simultaneously that generate both red and blue shifts in the resonant wavelength. Exposing the sensor to flow, thereby creating thermal boundary layers, washes away some of this "warm" water and replaces it with water at room temperature. In effect, this "cooling" of the water that has interacted with the optical mode produces a red shift. However, a more steep boundary layer increases the rate at which energy diffuses away from the resonator, lowering its temperature. The thermo-optical coefficient of glass is 1.3×10^{-5} K^{-1}, so cooling the resonator would yield a competing blue shift. Since silica absorbs so little light at 1310 nm, there is likely very little heat building up in the silica resonator compared to that due to absorption in the water. Accordingly, the net effect observed experimentally and shown in Fig. 6.3 upon flowing water around the WGM biosensor is a red shift because the removal of warm water from the mode is dominant.

A systematic study of this effect is ongoing. To date, this effect is unpublished, but would significantly impact the development of WGM biosensors at near-IR wavelengths that aim to cut costs by using inexpensive tunable lasers common to the telecommunications industry. This effect can be managed during a sensing experiment despite the notion that one would be unable to parse the respective contributions from biomolecular adsorption and fluid flow. This can be accomplished by collecting transient data while flowing

a protein solution until the signal reaches a steady state due to saturation of surface binding sites, followed by turning off the flow to reveal the steady-state signal due exclusively to the protein. The relative resonance shift from the beginning of the measurement until the system stabilizes in the absence of flow is the true endpoint datum.

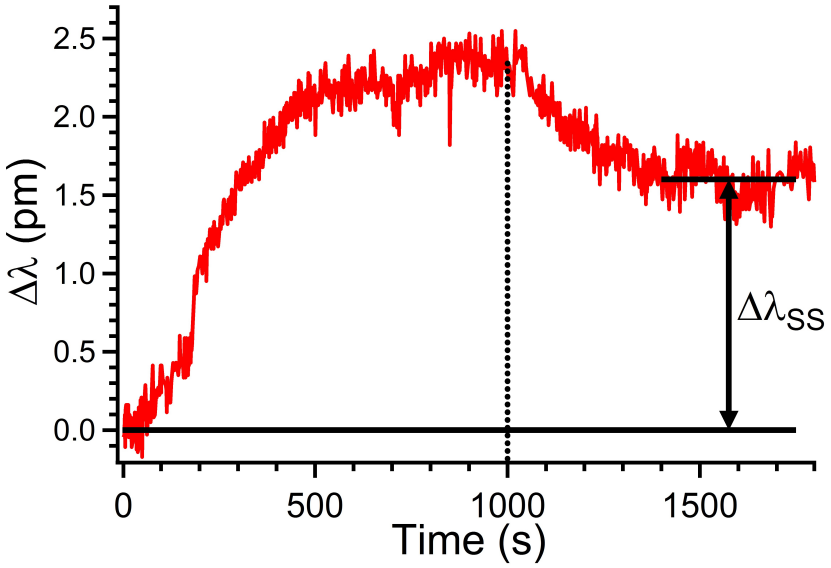

Figure 6.4: Detection of 100 fM Interleukin-2 in buffer using a toroid with Q=2.0×10^5, a flow rate of 50 μL/min, and a testing wavelength of 1310 nm. The dotted line marks when flow was shut off, and the endpoint resonance shift is marked as $\Delta\lambda_{SS}$

This method is demonstrated in Fig. 6.4 for the specific adsorption of 100 fM IL2. It clearly demonstrates how a single endpoint resonance shift, labeled $\Delta\lambda_{SS}$, is measured. It also shows the typical dual steady-state signal levels corresponding to the presence and absence of flow around the toroid. There is a signal-to-noise ratio of SNR>6:1, indicating that the true sensitivity of this assay is in the range of 1-10 fM for this analyte/buffer combination. As a point of reference, these data suggest that WGM optical biosensors outperform commercially available biosensor technologies such as surface plasmon resonance (SPR), which typically feature limits of detection (LODs) above 100 fM for label free assays.

Identical procedures were used to detect 8ip in solution as well. It was unclear beforehand how well WGM biosensors would be able to resolve specific adsorption of 8ip due to its small size. Fig. 6.5 shows the

cumulative resonance shifts measured during a series of 8ip sensing experiments where successively higher concentrations of the analyte were introduced into the flow cell. Just as in the case for IL2 detection, we measured the steady state value for $\Delta\lambda_{SS}$ in the absence of flow. The small ridges that appear in the signal within a single sensing experiment, more clearly visible in the inset to Fig. 6.5, correspond points when water drops fell off of the sample holder and caused vibrations in the air-water interface around the flow cell. These vibrations cause motion in the tapered fiber waveguide and, subsequently, coupling-induced resonance shifts as the amount of power in the cavity changes. Fig. 6.6a shows the isolated sensor response to the specific adsorption of 100 μm 8ip. Note that the analyte concentration is a factor of 10^6 higher than that in Fig. 6.4, but the signal is only a factor of 3 larger. Fig. 6.6(b) shows a portion of the dynamic range for the microtoroidal WGM biosensor at 1310 nm, but it allows us to project a LOD of roughly 1-10 pM based on the SNR of the measurent.

It is important to keep in mind that these experiments are the beginning of our efforts to demonstrate WGM biosensor utility for detection of biomarkers. Our results are encouraging, especially considering that we tested at a wavelength of 1310 nm (limiting our sensitivity) and still observed LODs below the relevant concentrations of these analytes in the body. Our current detection limits for 8ip are similar to the techniques currently in use (LCMS, fluorescence assays). We hope to perform these measurements using 633 nm light, which will likely show a 10-1000 fold improvement in sensitivity compared to the present work. This will also allow us to establish a superior sensing detection method for 8ip and create opportunities to apply WGM biosensors to analytes that may be of even more use in diagnosing disease but are present at too low of concentrations for current analytical techniques.

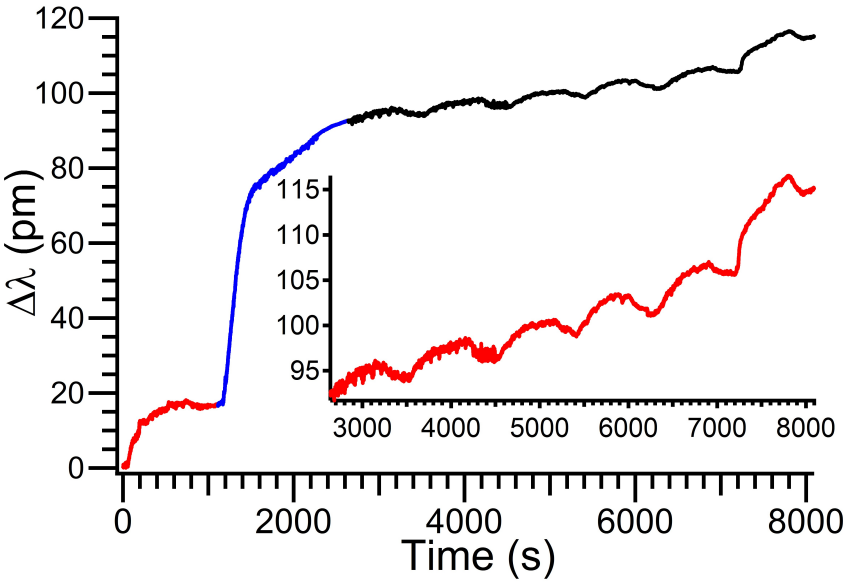

Figure 6.5: Detection of 8-isoprostane in buffer using a toroid with Q=4.2×10^5, a flow rate of 50 μL and a testing wavelength of 1310 nm. The data collection was stitched together to illustrate cumulative resonance shift. First Protein G (red) then polyclonal anti-8ip (blue) were allowed to adsorb. Next, six successively more concentrated 8ip solutions were flown into the cell (100 pM, 1 nM, 10 nM, 100 nM, 1 μM, and 10 μM). The inset expands this part of the curve for clarity.

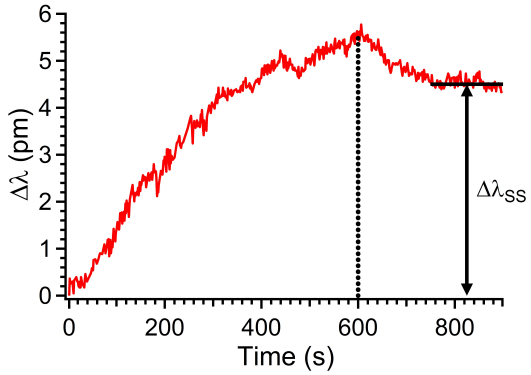

(a) Sensing 100 μM 8ip

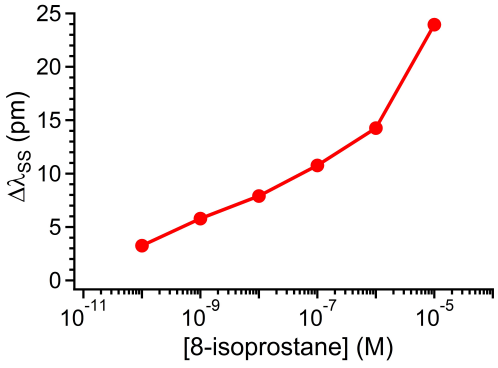

(b) Dynamic Range Sensing Data for 8ip

Figure 6.6: (a) This sample data for 100 μM 8ip appears to saturate before flow is turned off (dotted line), at which point it reaches a new steady state. The endpoint data sought in this measurement is the value of $\Delta\lambda_{SS}$, the true steady state resonance shift. (b) By collecting this endpoint resonance shift and plotting against the concentration of 8ip that elicited that shift, we have a partial dynamic range curve for this system.